HHS Public Access

Author manuscript

Nat Metab. Author manuscript; available in PMC 2020 April 01.

Published in final edited form as:

Nat Metab. 2019 October ; 1(10): 985–995. doi:10.1038/s42255-019-0110-3.

Muscle stem cell renewal suppressed by Gas1 can be reversed by GDNF in mice

Liangji Li[1,2], **Michelle Rozo**[1,2], **Sibiao Yue**[1,2], **Xiaobin Zheng**[2], **Frederick Tan**[2], **Christoph Lepper**[2,3], **Chen-Ming Fan**[1,2,*]

[1]Department of Biology, Johns Hopkins University, Baltimore, MD 21218

[2]Department of Embryology, Carnegie Institution for Science, Baltimore, MD 21218

[3]Department of Physiology and Cell Biology, College of Medicine, Ohio State University, Columbus, OH 43210

Abstract

Muscle undergoes progressive weakening and regenerative dysfunction with age due in part to the functional decline of skeletal muscle stem cells (MuSCs). MuSCs are heterogeneous but whether their gene expression changes with age and the implication of such changes are unclear. Here we show that in mice, Growth arrest-specific gene 1 (Gas1) is expressed in a small subset of young MuSCs with its expression progressively increasing in larger fractions of MuSCs later in life. Over-expression of Gas1 in young MuSCs and inactivation of Gas1 in aged MuSCs support that Gas1 reduces the quiescence and self-renewal capacity of MuSCs. Gas1 reduces Ret signaling, which is required for MuSC quiescence and self-renewal. Indeed, we show that the Ret ligand, Glial Cell-Derived Neurotrophic Factor (GDNF), can counteract Gas1 by stimulating Ret signaling and enhancing MuSC self-renewal and regeneration, thus improving muscle function. We propose that strategies aimed to target this pathway can be exploited to improve the regenerative decline of muscle stem cells.

Introduction

Heterogeneity of a stem cell population underlies a biological strategy to generate functional diversity. Stem cell heterogeneity can originate from distinct developmental origins, differential niche interactions, or dynamic epigenetic states[1–3]. For the MuSCs/progenitors, cell-lineage tracing in adult mice has identified two stem/progenitor cell origins marked by

*Author of correspondence: Chen-Ming Fan, fan@carnegiescience.edu.

Author contributions

L.L., M.R., and C.-M.F. conceptualized the projects, designed experiments, and wrote manuscript. L.L. and C.-M.F performed experiments, analyzed data, and made conclusions. S.Y. and C.L. assisted in FACS and ChIP-seq. C.L. provided mouse strains. X.Z. and F.T. performed bioinformatic analyses.

Competing financial interest

The authors declare no competing interests.

Data and/or Code Availability

All data that support the findings of this study and the custom code used during this study are available from the corresponding authors upon reasonable request.

the expression of Pax7 and Twist2[4,5]. While the *Twist2*$^{+}$-lineage contributes exclusively to type IIb/x myofibers[5], cell ablation studies conclude that the Pax7-expressing (Pax7^{+}) population is indispensable for general muscle regeneration[6–9]. Adult MuSCs/progenitors have also been characterized by various combinations of surface markers[10–12], and those with different marker combinations display different myogenic properties in vitro and after engraftment[10]. In addition, MuSCs expressing high versus low levels of a *Pax7* reporter (Pax7:nGFP) are functionally distinct in vitro and by serial transplantation[13]. These studies in juvenile and young adult mice demonstrate how heterogeneity underlies functional and cell type diversity. How variable levels of expression of a given gene within a cell population are governed to effect differential function is of intrigue.

During the aging process, MuSCs eventually decline in cell number and function[14,15]. Cultured aged MuSCs, relative to the young, have lower proliferation and self-renewal capacity, as well as higher propensity for differentiation[16,17]. However, it is unknown whether or how such decline is linked to changing heterogeneity in the stem cell population. When assessed as a whole population, young and aged MuSCs show substantial differences in gene expression and epigenetic state[18], reflecting a combined effect of age-associated changes in systemic factors, local niche environment and cell intrinsic properties. While this approach uncovers candidate MuSCs regulators based on averaged differences in expression level, it does not distinguish whether the difference is due to changes of gene expression levels in all cells or due to changes in the fraction of cells with the same expression level, or both. If a gene-specific MuSC sub-fraction exists, will the fraction change with age? Will such a gene impact MuSC function with time? If so, what is the underlying mechanism? Serendipitously, we answered these questions by studying the role of *Growth arrest-specific gene 1, Gas1*, which encode a GPI-anchored plasma membrane protein[19], in mouse MuSCs. We find that Gas1-expressing (Gas1^{+}) MuSC sub-population is dynamic and increases with age. Evidence is provided that functional decline of MuSCs is associated with Gas1 expression, in particular for their quiescence and self-renewal. We further link Gas1 to repressed Ret signaling, which is needed for robust MuSC function. Importantly, GDNF, a ligand for Ret, can counter the repressive action of Gas1 and enhance MuSC's regenerative function.

Results

Gas1 expression in the MuSC population changes with age

We had intended to explore a potential role for Gas1 in MuSC quiescence for it is a G0 indicator and can inhibit S phase entry when over-expressed in cell lines[20], and it was documented to be expressed in quiescent MuSCs[21]. Surveying Gas1 expression using a LacZ knock-in allele[22], we found that β-Gal reporter is expressed in a small fraction of young Pax7^{+} MuSCs, the fraction increases with age, and eventually almost all aged MuSCs are β-Gal^{+}(Fig. 1a; Supplementary Fig. 1a). The kinetics does not follow the timing of MuSC quiescence or aging: At 2 month (m) of age when MuSCs are quiescent, only ~40% of them are β-Gal^{+} (Supplementary Fig. 1b–d), whereas at 6 – 12 m when MuSCs are robust for regeneration, ~80–90% of them are already β-Gal^{+}. We used fluorescent activated cell sorting (FACS) to confirm Gas1^{+} versus Gas1^{-} subpopulations in young MuSCs, compared

to mostly Gas1$^+$ aged MuSCs; β-Gal faithfully follows Gas1 expression (Supplementary Fig. 1e,f). The kinetics of β-Gal$^+$ (i.e. Gas1$^+$) MuSCs may reflect a long maturation process that continues into aged state.

Gas1$^+$ MuSCs have inferior function than Gas1$^-$ MuSCs in vitro

If Gas1 expression merely reflects maturation timing without functional consequences, Gas1$^+$ and Gas1$^-$ MuSCs in young mice should be functionally equivalent. To evaluate this, we isolated β-Gal$^+$ and β-Gal$^-$ MuSCs from 2 m young mice, and found that the former displayed lower proliferation index and higher propensity to differentiate in culture, compared to the latter (Supplementary Fig. 1g–j). Thus, Gas1 is negatively associated with MuSC function in vitro. Yet, such association does not appear reflected in vivo as mature adults with the majority of Gas1$^+$ MuSC regenerate effectively. We therefore postulate that extrinsic factors exist in vivo to counter or mask the inferior properties of Gas1$^+$ MuSCs revealed in vitro.

Gas1 negatively impacts MuSC and muscle regeneration

To test whether *Gas1* plays an instructive role to MuSC dysfunction in vivo, we designed experiments in young and aged contexts when MuSCs are well known to be robust versus compromised, respectively. For forced pan-expression of Gas1 in young MuSCs, we used a *Pax7*$^{Cre\text{-}ERT2}$ (*Pax7*^{CE})-driven, tamoxifen (Tmx)-inducible strategy[7] for pan-expression of a Gas1 transgene in young MuSCs; hereafter referred to as Gas1EX (Fig. 1b; Supplementary Fig. 2a,b). MuSC activation and loss were found (Fig. 1c; Supplementary Fig. 2c,d,f). Ectopic expression of the differentiation marker MyoG was also observed (Fig. 1d; Supplementary Fig. 2e). We then injured the tibialis anterior (TA) muscles of Gas1EX mice by cardiotoxin (CTX). Smaller regenerative myofibers were observed, compared to the young control (Fig. 1e,f). Reduced Pax7$^+$ cells in Gas1EX regenerates were also found (Fig. 1c; Supplementary Fig. 2f). Thus, pan-expression of Gas1 in young MuSC population results in breaking quiescence, cell loss, and defective regeneration. These results indicate that forced Gas1 expression can drive MuSC dysfunction in young mice, presumably by overriding extrinsic counteracting factors postulated above.

Given that Gas1 is expressed in almost all aged MuSCs, we next examined whether inactivation of *Gas1* in MuSCs would improve regenerative function in aged mice. For this, we bred mice for Tmx-induced deletion of *Gas1* in Pax7$^+$ MuSCs in aged mice; hereafter referred to as Gas1KO (Fig. 1b; Supplementary Fig. 2b). Inactivation of *Gas1* in MuSCs helped to increase MuSC pool size in aged mice under sedentary condition (Fig. 1g; Supplementary Fig. 2g) - though still smaller than the MuSC pool size in the young. Compared to aged controls, Gas1KO muscles showed better regeneration, i.e. larger regenerated muscle fibers (Fig. 1h,i). Importantly, increased Pax7$^+$ cells were found after regeneration (Fig. 1g, Supplementary Fig. 2g), indicating that MuSC self-renewal is improved in Gas1KO mice. Thus, without Gas1 function in MuSCs, aged muscles regenerate better, indicating that Gas1 contributes to their dysfunction.

Gas1 compromises MuSC self-renewal cell-autonomously

The above in vivo data may be explained by changes in the number of MuSCs in Gas1EX and Gas1KO models. To determine whether there is also an intrinsic change in self-renewal, we analyzed myogenic cell fates ex vivo using the single myofiber (SM) assay[23] in which MuSCs were associated with intact wild type fibers. Aged Gas1KO MuSCs increased $Pax7^{+}MyoD^{-}$ self-renewed fraction, compared with aged controls (Fig. 1j; Supplementary Fig. 3a,b). Similar to aged controls, young Gas1EX MuSCs generated a larger $Pax7^{-}MyoD^{+}$ differentiation-committed fraction, compared with young controls. These data corroborate with in vivo data and support Gas1 causes a defect in MuSC self-renewal, distinct from its role in muscle terminal differentiation studied in C2C12 cells[24].

Regenerated muscles of Gas1EX and Gas1KO have reduced force

We further assessed regenerated muscle strength in young Gas1EX and aged Gas1KO mice by measuring single-twitch and tetanus forces in situ at 1 m post injury (1 mpi; Supplementary Fig. 3d). Correlating with histological data (Supplementary Fig. 3c), regenerated young Gas1EX muscles showed marked diminution in both forces, relative to young controls, whereas regenerated muscles of aged Gas1KO mice showed enhanced forces relative to aged controls (Fig. 1k, Supplementary Fig. 3e).

Transcriptome and epigenome of Gas1EX and Gas1KO MuSCs

Given that reduced number and self-renewal capacity of MuSCs are features of aging, we wondered whether Gas1 also leads to changes of biological processes in MuSCs that are related to those particular aspects of aging. For this, we performed RNA-seq of FACS-purified young, aged, young Gas1EX, and aged Gas1KO MuSCs (Fig. 2; Supplementary Fig. 4); microarray data were used to compare wild type young and aged MuSCs previously[19]. Multidimensional scaling (MDS) segregates young and aged control MuSC transcriptomes (Fig. 2a), and differentially expressed (DE) genes between aged and young control MuSCs provides aging-related gene sets. Differential gene expression largely correlates with differential levels of active chromatin mark H3K4me3 at gene promoters assessed by ChIP-seq (Fig. 2c), indicating that expression changes occur at the level of transcription; an example for the *Ret* locus is shown (Fig. 2d). Young Gas1EX and aged Gas1KO MuSC transcriptomes are grouped away from the young and aged controls, respectively, by MDS (Fig. 2a). Ninety-three of 120 up-regulated genes and 131 of 158 down-regulated genes in young Gas1EX MuSCs (compared to the young control) overlap with correspondingly up- and down-regulated aging-related DE gene sets (Fig. 2b), revealing the similarity between young Gas1EX and aged control MuSCs. When aged control is compared to aged Gas1KO, significant overlap with aging-related DE gene sets in the same directions of change are noted, supporting that Gas1KO transcriptome is of younger signature. Considering young Gas1EX and aged Gas1KO MuSCs encounter niche environment and physiological parameters differing from the aged and young control MuSCs, respectively, the large overlaps by transcriptome comparison are remarkable. Gene set enrichment analysis (GSEA) revealed a strong correlation between young Gas1EX and aged control MuSCs, including enrichment of inflammatory response and cell cycle genes (Fig. 2e). Categorizing DE genes among the four data sets according to the hallmarks of

aging[25] (Fig. 2f), we noted extracellular signaling, nutrient sensing, and cell adhesion genes. Several genes implicated in systemic or MuSC aging are present, e.g. IGF1[26] and Fibronectin (Fn1)[27]. Gas1 has been implicated in the Hedgehog (HH) pathway during embryogenesis[22], but no changes in HH downstream genes were found. Shared molecular signatures between young Gas1EX and aged MuSCs potentially inform players downstream of Gas1 that effect quiescence and self-renewal defects observed in aged MuSC.

Ret is downstream of Gas1 for MuSC quiescence and renewal

Among the DE genes, we were intrigued by reduced mRNA and H3K4me3 levels of *Ret* in aged and young Gas1EX MuSCs (Fig. 2d, 3a) as there are reported physical association between Ret and Gas1 in cultured cell lines[25–27]. *Ret* encodes a receptor tyrosine kinase (RTK) which is a common signaling component for glial cell line-derived neurotrophic factor (GDNF) family of ligands, and plays many roles in the nervous system, including in motor axons that effect muscle contraction[28]. To elucidate its role in MuSC, we first utilized an engineered conditional *Ret* allele (Ret^{flox}) with a change in the kinase domain that allows for specific binding and inhibition by the small molecule 1NM-PP1[29]. We found that 1NM-PP1 decreased renewal and increased differentiation of MuSCs ex vivo, compared to mock-treatment controls (Fig. 3b); 1NM-PP1 showed no effect on MuSCs not carrying this Ret^{flox} allele (Supplementary Fig. 5a). Regorafenib[30], a broad RTK inhibitor that also targets Ret, yielded a similar result (Supplementary Fig. 5b). To examine the role of *Ret* in MuSCs in vivo, we inactivated *Ret*[29] in young $Pax7^+$ MuSCs (hereafter referred to as 'RetKO', Fig 3c). RetKO mice showed a decline in MuSC number without injury (Fig. 3d; Supplementary Fig. 5c). After injury, RetKO mice were defective in regeneration as reflected by reduced fiber size of repaired muscles (Fig. 3e; Extended Data Fig.5d,e). Furthermore, both muscle injury and SM assay revealed a reduction in renewed $Pax7^+$ cells (Fig. 3d, f; Supplementary Fig. 5c). Thus, phenotypes of RetKO parallel those of Gas1EX (whose MuSCs express low level of *Ret*), leading us to propose that reduced *Ret* levels underlie Gas1EX phenotype.

Gas1EX and RetKO models do not support muscle hypertrophy

We further evaluated Gas1EX and RetKO mouse models in the context of compensatory hypertrophic growth of the Plantaris muscle after synergistic ablation (SA) of Soleus and Gastrocnemius muscles[11,31] (Fig. 4a). As expected, after SA, control animals showed significant increases in Plantaris myofiber size and in myofibers with centrally located nuclei. However, the two experimental models did not show obvious changes (Fig. 4b, c; Supplementary Fig. 6a). To elucidate the underlying causes, we probed for Pax7 to assess stem cell pool changes. Relative to controls, both mouse models showed decreased $Pax7^+$ MuSCs, with or without SA (Fig. 4d, e), consistent with their loss in quiescence and compromised renewal after activation. Furthermore, EdU^+ myonuclei and $Pax7^+EdU^+$ SCs were found to be increased in the Plantaris muscles after SA, but the increases are considerably lower in the two models than in the control (Supplementary Fig. 6b, c). These data indicate that compensatory responses were mounted in these two models, but insufficient to cause a significant change in myofiber size. Accordingly, SA-operated hindlimbs of the two models showed weaker grip-strength than those of control mice (Fig. 4f). We note that the requirement of MuSCs for Plantaris hypertrophy after SA has been controversial[11,31]. Nevertheless, our SA and CTX-injury results together support the

negative role of Gas1 and positive role of Ret in MuSCs for hypertrophic growth and regeneration, respectively.

Gas1 antagonizes Ret signaling in MuSC

Biochemical interaction between Gas1 and Ret is ill-defined and how Gas1 modulates Ret activity is controversial[32–34]. The biological relevance of their interaction is also unclear. To establish a relevance in the context of MuSC, we first determined if physical association with Ret is necessary for Gas1 to impede MuSC self-renewal. We generated three deletion mutants of Gas1 and found that its first cysteine-rich domain (domain 1) was essential for Ret binding by co-immunoprecipitation (Fig. 5a). Transient expression of Gas1 in young MuSCs on the SM was sufficient to reduce self-renewal, whereas domain 1 deletion mutant of Gas1 had no effect (Fig. 5b, c). Therefore, Gas1's ability to reduce MuSC self-renewal depends on its Ret-interacting domain.

To extend the above finding, we assayed for phosphorylation of RetY1062 (pRet) in various biological contexts. Approximately 40% of the young MuSCs were $pRet^{+}$. By contrast, most young Gas1EX and aged MuSCs are $pRet^{-}$ (Fig. 6a; Supplementary Fig. 7). Using the Proximal Ligation Assay (PLA), we detected co-localization of Gas1 and Ret (as foci) in young and aged MuSCs, which correlated with Gas1 expression (Fig. 6b, c). These results together are consistent with a model that Gas1 directly associates with Ret to suppress signaling in MuSCs.

GDNF reverses the repressive effect of Gas1 on Ret signaling

We next asked whether it is possible to reverse the negative effect of Gas1 impinged on Ret. GDNF is a natural ligand for the Ret-GFRα1 dimer[28]. Among four members of the GFRα family, GFRα1 is expressed the highest whereas GFRα4 is not detected in MuSCs (our RNA-seq data). Application of GDNF to MuSCs on SM isolated from young and aged mice resulted in a considerable increase of the $Pax7^{+}MyoD^{-}$ self-renewed fraction (Fig. 6d, e). By contrast, Persephin (PSPN), a ligand for the Ret-GFRα4 dimer[28], had no effect (Supplementary Fig. 8a). Consistently, GDNF increased the $pRet^{+}$ fractions of young and aged MuSCs (Fig. 6a). GDNF also increased the $pRet^{+}$ (Fig. 6a) and $Pax7^{+}MyoD^{-}$ fractions (Supplementary Fig. 8b) of young Gas1EX MuSCs, indicating a reversal of Gas1-mediated inhibition of Ret. Furthermore, GDNF reduced Gas1-Ret PLA foci in young and aged MuSCs (Fig. 6c). Thus, GDNF can stimulate Ret signaling, reduced Gas1-Ret interaction, and reverse the inhibitory effect imposed by Gas1, in MuSCs.

The above results inspired us to test whether intramuscular injection of GDNF could rescue the defects in the Gas1EX model. Indeed, we observed improvements in regenerative myofiber size and muscle forces in GDNF-treated young Gas1EX muscles (Supplementary Fig. 8c–g). As a control, young RetKO failed to respond to GDNF treatment, both ex vivo and in vivo (Supplementary Fig. 9). Our proposal that functional decline of MuSCs is associated with Gas1's inhibitory effect on Ret signaling makes the prediction that GDNF should also overcome Gas1, stimulate Ret signaling, and enhance the function of MuSCs in naturally aged mice. We were pleased to find that not only aged muscle regeneration and regenerated muscle forces were improved by intramuscular GDNF injection (Fig. 6f,g,j,k,),

but also the number of Pax7^{+} MuSCs (Fig. 6h,i). While GDNF likely has other cell targets, our data collectively support that it can act on aged MuSCs to reverse dampened Ret signaling associated with Gas1 expression and improve regenerative function.

Discussion

Aged skeletal muscle is featured by decreased muscle mass, a chronic physiological condition referred to as 'sarcopenia'. Concomitantly, MuSCs display age-associated decline in number and function for regeneration[14,15,35]. While MuSC is essential for muscle regeneration, aging-associated sarcopenia appears independent of MuSC[36]. Here we provide evidence that Gas1 drives functional decline of MuSCs by reducing their stemness in quiescence and during regeneration. Several observations indicate that the role of Gas1 is masked in young and mature mice: 1) young Gas1^{+} MuSCs are functionally interior to Gas1^{-} MuSCs in vitro, but together they regenerate muscle robustly in vivo; 2) The majority of MuSCs expresses Gas1 in mature mice when muscle regeneration is still effective; 3) Yet, the negative role of Gas1 can be revealed by over-expression in young MuSCs. We suggest that active GDNF-Ret signaling is the 'masking' pathway that prevents Gas1 from action in young and mature adults. In chronologically aged mice, Gas1's inhibitory role on quiescence and self-renewal becomes realized to reduce *Ret* transcription and pRet levels, but reversible by GDNF. Given the existing[32–34] and the data provided here for these 3 components, we propose that mutually antagonistic but titratable interactions between them explain why the aged-independent role of Gas1 for MuSC renewal is revealed in an age-specific manner. Thus, MuSCs are 'pre-marked' by Gas1 expression gradually from youth to maturation, for their destined functional decline in aging. As reduced renewal is part of MuSC aging, the transcriptome changes driven by Gas1 most likely reflect this aspect of functional decline. Gas1 over-expression also reduces *Ret* transcription in the young, suggesting a feedforward mechanism from reducing Ret signaling to reduced *Ret* transcription in MuSCs, as seen in aged MuSCs. We cannot exclude that additional factors may contribute to masking Gas1 function in the adult, and that GDNF may target other cell types than MuSCs in the regenerative process.

Contrast to increased Wnt[37] and Tgfβ[38] systemically and FGF2 locally[16] as extrinsic aging influences on MuSCs, reduced Ret signaling is driven by intrinsic expression of Gas1. These well-documented aging factors for MuSCs appear active in Gas1KO model, hence their transcriptome change towards the young is partial and their MuSC pool size is smaller than that in the young – even though the regeneration is substantially improved. It is worth noting that Ret is also important for motor axon regeneration[39] and synaptic maturation[40], whereas GDNF expression is elevated in newly regenerated muscle fibers[41]. The shared usage of GDNF-Ret signaling by MuSCs and motor axons during muscle regeneration signifies a coordinated biological strategy for functional muscle restoration. Extending our findings, we devised a proof of principle method to improve muscle regeneration by intramuscular delivery of GDNF, a natural biological factor. This contrasts to most studies using technically demanding in vitro manipulations to improve MuSCs, which are then transplanted. Future studies and translation of our results to humans will be of importance. Methods to manipulate endogenous levels of Gas1 and Ret in MuSCs, or levels of GDNF

produced by the muscle, may also be considered as therapeutic means for improving muscle regeneration.

Methods

Mouse strains.

The *Gas1*^{LacZ} mice[22], *Pax7*$^{\text{cre-ERT2}}$ (referred to as *Pax7*^{CE} in legends; B6;129-*Pax7*$^{\text{tm2.1(cre/ERT2)}}$*Fan*/J) mice[4], and *Gas1*^{flox} mice[42] have been described. The *R26*$^{\text{YFP}}$ (B6.129X1-*Gt*(*ROSA*)*26Sor*$^{\text{tm1(EYFP)}}$*Cos*/J) mice[43] and *Ret*$^{\text{flox}}$ (STOCK Ret<tm1.2Ddg>/J) mice[29] were obtained from the Jackson Laboratory (JAX). Whenever YFP was included for assay, the *R26*$^{\text{YFP}}$ allele was included in the background for Pax7^{+} MuSC lineage marking. The Gas1 conditional pan-expression (Gas1EX) allele, *R26*$^{\text{CAG-Gas1}}$, generated for this work is detailed in Supplementary Fig.2a. The Pax7-GFP knock-in allele, *Pax7*$^{\text{Avi−2A-GFP}}$ will be described by C. Lepper in a separate study. All the above mice are mixed background. C57BL/6 mice were used as wild-type (WT) mice. For young versus aged comparisons, mice were used at 2–3 month of age (young) or 18–24 month of age (aged). Both sexes were used for all experiments except for next generation sequencing experiments, where female animals were used. Animal experiments in this study were performed following the ethical regulations by Office of Laboratory Animal Welfare (OLAW), and in accordance with protocols approved by the Institutional Animal Care and Use Committee (IACUC) of the Carnegie Institution for Science (Permit number A3861–01).

Tamoxifen regimen, muscle injury, EdU and GDNF administration.

Mice were given tamoxifen (Tmx, 20 mg/ml in corn oil; Sigma) at 4 mg per 40 g body weight intraperitoneally for 5 consecutive days. For young groups, unless noted otherwise, assays were conducted 1 m after Tmx regimen. For aged groups, assays were conducted 18 m after Tmx regimen. For muscle injury, experimental and corresponding control mice were anaesthetized with isoflurane, their tibialis anterior (TA) muscle was injected with 50 μl of 10 μM cardiotoxin (CTX; Sigma) using an insulin syringe (U-100; Becton Dickinson), and harvested at post injury (pi) time points (stipulated as ‘d’ for day and ‘m’, for month) stated in the text and legends. For short-term daily in vivo proliferation, 5-ethynyl-2′-deoxyuridine (EdU; Life Technologies) was given by intraperitoneal injection at 0.1 mg per 20 g bodyweight per injection and muscle harvested as specified in legends. For in vivo GNDF treatment, TA muscles received 2 × 10 μl GDNF (50 ng/μl in PBS, PeproTech) at 2 and 4 dpi and were harvested at 14 dpi. For TA muscles harvested at 1 mpi, an extra dosage was administrated at 14 dpi. Phosphate buffered saline (PBS) was used for mock-injection for control.

Muscle sample processing.

TA muscles (in CTX muscle injury assay) or Plantaris muscles (see Synergist ablation below) were harvested, fixed for 10 min in ice cold 4% paraformaldehyde (EMS) in PBS, sequentially changed through 10%, 20% and 30% sucrose/PBS overnight, embedded in OCT, frozen in isopentane (Sigma)/liquid nitrogen, and stored at –80 °C freezer until cryo-sectioning. Cross-sections (10 μm) of the muscle mid-belly region were stained with

Haematoxylin and Eosin (H&E; Surgipath), or used for immunostaining and EdU reactions (see below).

MuSC isolation by FACS and myoblast culture.

MuSCs were isolated following the previously described protocol[44] with slight modifications. Briefly, for MuSC preparation, skeletal muscles were dissected and incubated in 0.2% Collagenase Type I (Sigma) in Ham's F-10 Nutrient Mix (F-10; Gibco) at 37 °C with gentle shaking for 1.5 h followed by centrifugation and wash. Tissues were then incubated in 0.2% Dispase (Gibco) in F-10 at 37 °C with gentle shaking for 0.5 h. Cells were then gone through 20-gauge needles for dissociation and filtered through 40 μm cell strainer (VWR) and wash. For surface maker labeling, cell were incubated with DAPI and fluorophore-conjugated antibodies against CD45, CD31, Sca-1 and Vcam, at 4 °C for 0.5 h. After wash, cells were subjected to fluorescence-activated cell sorting (FACS) using the ARIA III sorter (BD Biosciences) and data were collected by BD FACSDiva software. Isolated mononuclear MuSCs were collected in Trizol (Thermo Fisher Scientific) for RNA-seq (see below), in F-10 with 10% horse serum (HS) for ChIP-seq (see below), cytospun for immunostaining, or replaced to MuSC culture medium (20% Fetal Bovine Serum (FBS), 5% HS, 1% Pen/Strep, 1% Glutamax (Gibco), 0.1% chick embryo extract (MP biomedicals) in DMEM (Gibco)) for culture. They were plated on Matrigel-coated dishes (Corning, 354248; 30 min at 37 °C), and cultured at 37 °C in tissue culture incubators with 5% CO_2. For live detection of β-Gal activity, cells were subjected to reaction using in vivo lacZ β-Galactosidase Intracellular Detection Kit (MarkerGene) following the manufacturer's guidelines and FACS isolated. For EdU labeling, EdU (10 μM) was added to MuSC culture medium for 2.5 h before harvesting for assay.

Single myofiber (SM) isolation, transfection, and culture.

SMs with associated MuSCs were isolated from extensor digitorum longus (EDL) muscles[23] by 1.5 h digestion in 0.2% Collagenase Type I in DMEM at 37 °C. The digested EDL muscle was then transferred to petri dishes containing DMEM, 1% Pen/Strep, and 1% Glutamax for mechanical dissociation to release individual myofibers. Isolated myofibers were subjected to direct fixation for immunostaining, or transferred to serum-coated Petri dishes for culture (SM culture medium: 10% FBS, 1% Pen/Strep, 1% Glutamax in DMEM). Pending on the assays, myofibers were cultured for different lengths of time before fixation and downstream assays. For pRet analysis and PLA assay (see below), myofibers were cultured for 24 h. Phosphatase Inhibitor Cocktail Set II (Calbiochem) was used as directed during fixation. For self-renewal assays with Pax7 and MyoD expression, 96 h cultures were used. For SM transfection, isolated myofibers were transfected with VSV-G-tagged full-length Gas1, Gas1-domain 1-truncation mutant, or GPI-anchored-YFP using TransfeX (ATCC) at 1:3 DNA(μg):TransfeX(μl) ratio. Twelve h after transfection, fresh SM culture medium was added and myofibers were cultured for total of 96 h at 37 °C, 5% CO_2 for self-renewal assays. For Ret signaling inhibition, 1NM-PP1 (10 nM and 100 nM, EMD Millipore) and Regorafenib (10 nM, Selleckchem) was added to SM culture medium for samples from $Ret^{flox/flox}$ mice and control mice, respectively. GDNF (20 ng/ml; PeproTech) or PSPN (as specificity control, 20 ng/ml; ProSpec) was directly added to the culture.

Medium was changed daily with the same concentration of inhibitors or recombinant factors until assay.

Immunostaining.

TA or Plantaris muscle sections, SMs or cytospun MuSCs were fixed for 10 min in 4% paraformaldehyde, permeabilized with 0.1% Triton-X-100 (Sigma)/PBS for 10 min at room temperature (RT), rinsed with wash buffer (0.05% Triton-X 100/PBS), treated with blocking buffer (10% Normal Goat Serum (Genetex) and 1× carbo-free blocking solution(Vector)) for 1 h, prior to incubation with primary antibodies (see Supplementary Table) diluted in blocking buffer overnight at 4 °C. Samples were then washed with wash buffer and incubated with appropriate Alexa-Fluor-conjugated secondary antibodies (1:1,000, Life Technologies) and in blocking buffer for 1 h at RT. After wash and incubation with 4′,6-diamidino-2-phenylindole (DAPI) at1 μg/ml for 5 min, samples were mounted with Fluoromount-G (SouthernBiotech) and coverslip (VWR). For EdU detection, the Click-iT reaction kit (Life Technologies) was used prior to incubation in DAPI according to manufacturer's recommendations.

Force measurement.

In situ force measurements of TA muscles were conducted as previously described[45,46], and the data were analyzed using the 1300A Whole Animal System (Aurora Scientific) using ASI 610A Dynamic Muscle Control v5.420 software. Mice were anaesthetized with isoflurane and placed on isothermal stage. Intact TA muscles were dissected and constantly immersed in Ringer's solution (homemade). Single twitch or tetanic contractions were elicited with electrical stimulations applied by two electrodes placed on either side of the muscle. In all experiments 0.2 ms pulses at 10 V supramaximal voltage were used. Muscle optimal length (Lo) that allows a maximum isometric twitch force (P_t) was determined by a series of twitch contractions with small variations of the muscle tension. To obtain maximum isometric tetanic force (P_o), muscles were stimulated for 300 ms at different frequencies from 50 to 200 Hz. A 1 min recovery period was allowed between stimulations. Muscle wet weight and Lo were used to calculate the cross-sectional area (CSA) of the TA muscle for normalization to obtain specific isometric twitch force sP_t (kN/mm^2) and sP_o (kN/mm^2).

RNA-seq and analysis.

For each condition, 30,000 of fresh isolated MuSCs by FACS were lysed in Trizol reagent. RNA was isolated using the Direct-zol RNA Kit (Zymo). cDNA was generated and amplified using TruSeq RNA Library Preparation Kit v2 (Illunima) and amplified with ThruPLEX DNA-seq Kit (Rubicon). Sequencing was carried out on an Illumina Nextseq-500 to generate single-ended 75 bp reads, which were aligned to the mouse genome (mm9) using TopHat (v2.1.0). Expression measurement of each gene was calculated from the resulting alignment bam file by HTseq against the GENCODE annotation vm1. Differentially expressed genes were determined using edgeR with FDR cutoff of 0.05. MDS-plots were also generated using the edgeR package. GSEA[47] analysis was performed using ranked fold change values with hallmark gene sets database (h.all.v6.2.entrez.gmt).

ChIP-seq and analysis.

Low-input ChIP-seq for fresh isolated MuSCs by FACS was performed following the previously described protocol[48] with slight modifications. In brief, for each condition, 30,000 MuSCs were fixed with 1% formaldehyde/PBS for 10 min at RT, before quenching the reaction with 1/20 volume of 2.5 M glycine for 5 min at room temperature and mixing with ~5×10^8 DH5α *E.coli* (as carrier). Cell lysis, chromatin isolation and digestions were done using the EZ Nucleosomal DNA Prep Kit (Zymo) followed by further chromatin shearing and releasing using Bioruptor Pico (Diagenode) with 6 cycles of 30 s on/off sonication. The immunoprecipitations were performed using anti-H3K4me3 antibody (EMD Millipore, 07–473, 1:1,000) at 4 °C overnight. The immunoprecipitated DNA was then bound to Protein G Dynabeads (Thermo Fisher Scientific) for 2 h at 4 °C, followed by serial washes, proteinase K digestion, and purification by DNA Clean & Concentrator kit (Zymo). DNA libraries were prepared using ThruPLEX DNA-seq Kit (Rubicon) and sequenced on an Illumina HiSeq 2000 machine to generate single-ended 75bp reads. ChIP-seq reads were aligned to mouse genome (mm9) using Bowtie (version 1.1.2). 2 mismatches were allowed for the alignment and only uniquely mapped reads were allowed (parameters -v 2 -m 1). Promoter correlations for H3K4me3 enrichments are plotted as log2 of the average read density within 2 Kb up and downstream of TSS. H3K4me3 peaks were called by MACS with *p*-value threshold of 10^{-5}.

Data repository.

All sequencing data has been deposited into the NCBI SRA database (accession code: PRJNA494728).

Synergist ablation surgery.

Muscle overload of the Plantaris muscles was induced by surgical removal of synergist muscles (Gastrocnemius and Soleus)[11,31]. Briefly, mice were anesthetized with IP injection of Avertin (2.5% tribromoethanol) at a dosage of 20 μL/g of body weight. Back of the lower hindlimb was incised to expose the synergist muscles. The tendons of gastrocnemius and soleus muscles were cut following by the removal of the distal portion (~ 50%) of these muscles, with the Plantaris muscle intact. The incision was then sutured and the wound disinfected. Synergistic ablations (SA) were performed unilaterally, and the mice were subjected to muscle overload for two weeks. EdU (5 μg/gram body weight) were intraperitoneal injected daily after the surgery until harvest.

Grip Strength.

Mice were held at the base of the tail over a base plate, in front of a grasping grid of the GSM Grip-Strength Meter (Ugo Basile). The grip strength of hindlimbs were measured via allowing the mice to grab the grid and pulling the mice backward gently until release, using Ugo Basile DCA software. 5 trials of peak force were recorded for each hindlimb and the average was used for quantification. A 5 min interval for recovery was allowed between each trail. Data are presented as relative fold change of mean grip strength of the operated leg relative to that of sham control.

Proximity ligation assay (PLA).

PLA for Gas1 and Ret on MuSCs were performed with Duolink In Situ Red kit (Sigma) following the manufacturer's guidelines. In brief, SM were fixed for 10 min in 4% paraformaldehyde, permeabilized with 0.1% Triton-X-100/PBS for 10 min at RT, and blocked with Duolink Blocking Solution for 2 h. Myofibers were then incubated with primary antibodies against Gas1 (goat, R&D, AF2644, 1:50) and Ret (rabbit, Alomone, ANT-025, 1:50) diluted in Duolink Blocking Solution at 4 °C overnight. Omitting either primary antibody resulted in no signal. PLA reactions were subsequently carried out using Duolink PLA probes for goat and rabbit and Duolink In Situ Detection Reagents Red. After washes, myofibers were stained for Pax7 using the moncoloncal Ab (DSHB), followed by an Alex-488 anti-mouse IgG1 secondary antibody (Invitrogen) and DAPI, and then mounted in ProLong Diamond Antifade Mountant (Thermo Fisher Scientific). Quantification of PLA was performed by counting PLA foci number per MuSC.

Co-immunoprecipitation.

HEK293T cells (Clontech, tested negative for mycoplasma contamination by MycoProbe Mycoplasma Detection Kit (R&D Systems)) were transfected with pcDNA3–3xFLAG-Ret and/or pAP-VSV-G-Gas1/Gas1-domain-truncated mutants by lipofectamine2000 (Invitrogen) for 24 h according to manufacturer's guidelines. Cells were lysed in lysis buffer (50mM Tris pH 8.0, 150mM NaCl, 0.5% Digitonin (Sigma), and protease inhibitors) for 1 h at RT. Cell lysates were cleared by centrifugation, and subjected to immunoprecipition by either anti-FLAG M2 Affinity Gel (Sigma) or anti-VSV-G Agarose Conjugate (Sigma) for 2 h at 4 °C. Affinity matrixes were washed and eluted in 2X SDS-PAGE sample buffer for Western blotting using anti-FLAG (Sigma) and anti-VSV-G antibodies (Invitrogen). Western results were obtained by Odyssey CLx Near-Infrared Fluorescence Imaging System (Li-Cor) using Image Studio 5 software.

Microscopy and image processing.

Images of H&E stained muscle sections were captured from Nikon 800 microscope with 20× Plan Apo objectives and Canon EOS T3 camera using EOS Utility image acquisition software. Fluorescent images of muscle sections and single myofibers were either captured by Nikon' Eclipse E800 microscope equipped with 20×/0.50 Plan Fluor, 40×/0.75 Plan Fluor, and 100×/1.3 Plan Fluor oil objectives and Hamamatsu digital camera C11440 using MetaMorph Microscopy Automation and Image Analysis Software, or captured by Leica SP5 confocal microscope equipped with 63×/1.4 Plan Apo oil objective using Leica image acquisition software. Same exposure time was used and images were processed and scored with blinding using ImageJ64. If necessary, brightness and contrast were adjusted for an entire experimental image set. Cell number, fiber diameter, fiber number, and fiber cross sectional area were determined using ImageJ64.

Statistical analyses.

Quantitative values are expressed as the mean ± standard deviation (s.d.). Statistical differences between two groups were determined by t-test for two-tailed unpaired comparison (refer to legends of Figs. 1–4). Additional statistical tests are detailed in legends

of Figs. 1–4. $P < 0.05$ was determined to be significant for all experiments. All experiments have been done at least twice with the same results. All statistical analyses were performed with Excel software or GraphPad Prism software. For mouse experiments, no specific blinding method was used but mice in each sample group were selected randomly. No statistical methods were used to predetermine sample size. No animal has been excluded from analysis and no randomization method has been applied in this study.

Reporting Summary.

Further information on research design is available in the Nature Research Reporting Summary linked to this article.

Data availability

All data that support the findings of this study are available from the corresponding authors upon request.

Supplementary Material

Refer to Web version on PubMed Central for supplementary material.

Acknowledgement

We thank the Fan lab members and Dr. Y. Zheng for comments, and E. Dikovsky, the mouse facility team, and S. Satchell for technical assistance. We especially thank Dr. T. Cheung for sharing the FACS protocol. L.L. is supported by Carnegie Institution of Washington (CIW), M.R. was supported by a predoctoral fellowship from the NIH (HD075345), and C.-M.F. is supported by NIH (R01AR060042, R01AR071976, and R01AR072644) and CIW.

References

1. Merkle FT, Mirzadeh Z & Alvarez-Buylla A Mosaic organization of neural stem cells in the adult brain. Science 317, 381–384 (2007). [PubMed: 17615304]
2. Lo Celso C, et al. Live-animal tracking of individual haematopoietic stem/progenitor cells in their niche. Nature 457, 92–96 (2009). [PubMed: 19052546]
3. Hayashi K, de Sousa Lopes SMC, Tang F, Lao K & Surani MA Dynamic equilibrium and heterogeneity of mouse pluripotent stem cells with distinct functional and epigenetic states. Cell stem cell 3, 391–401 (2008). [PubMed: 18940731]
4. Lepper C, Conway SJ & Fan CM Adult satellite cells and embryonic muscle progenitors have distinct genetic requirements. Nature 460, 627–631 (2009). [PubMed: 19554048]
5. Liu N, et al. A Twist2-dependent progenitor cell contributes to adult skeletal muscle. Nature cell biology 19, 202–213 (2017). [PubMed: 28218909]
6. Lepper C, Partridge TA & Fan CM An absolute requirement for Pax7-positive satellite cells in acute injury-induced skeletal muscle regeneration. Development 138, 3639–3646 (2011). [PubMed: 21828092]
7. Murphy MM, Lawson JA, Mathew SJ, Hutcheson DA & Kardon G Satellite cells, connective tissue fibroblasts and their interactions are crucial for muscle regeneration. Development 138, 3625–3637 (2011). [PubMed: 21828091]
8. McCarthy JJ, et al. Effective fiber hypertrophy in satellite cell-depleted skeletal muscle. Development 138, 3657–3666 (2011). [PubMed: 21828094]
9. Sambasivan R, et al. Pax7-expressing satellite cells are indispensable for adult skeletal muscle regeneration. Development 138, 3647–3656 (2011). [PubMed: 21828093]

10. Sherwood RI, et al. Isolation of adult mouse myogenic progenitors: functional heterogeneity of cells within and engrafting skeletal muscle. Cell 119, 543–554 (2004). [PubMed: 15537543]
11. Gilbert PM, et al. Substrate elasticity regulates skeletal muscle stem cell self-renewal in culture. Science 329, 1078–1081 (2010). [PubMed: 20647425]
12. Cheung TH, et al. Maintenance of muscle stem-cell quiescence by microRNA-489. Nature 482, 524–528 (2012). [PubMed: 22358842]
13. Rocheteau P, Gayraud-Morel B, Siegl-Cachedenier I, Blasco MA & Tajbakhsh S A subpopulation of adult skeletal muscle stem cells retains all template DNA strands after cell division. Cell 148, 112–125 (2012). [PubMed: 22265406]
14. Sousa-Victor P, Garcia-Prat L, Serrano AL, Perdiguero E & Munoz-Canoves P Muscle stem cell aging: regulation and rejuvenation. Trends Endocrinol Metab 26, 287–296 (2015). [PubMed: 25869211]
15. Brack AS & Munoz-Canoves P The ins and outs of muscle stem cell aging. Skelet Muscle 6, 1 (2016). [PubMed: 26783424]
16. Chakkalakal JV, Jones KM, Basson MA & Brack AS The aged niche disrupts muscle stem cell quiescence. Nature 490, 355–360 (2012). [PubMed: 23023126]
17. Cosgrove BD, et al. Rejuvenation of the muscle stem cell population restores strength to injured aged muscles. Nature medicine 20, 255–264 (2014).
18. Liu L, et al. Chromatin modifications as determinants of muscle stem cell quiescence and chronological aging. Cell reports 4, 189–204 (2013). [PubMed: 23810552]
19. Del Sal G, Ruaro ME, Philipson L & Schneider C The growth arrest-specific gene, gas1, is involved in growth suppression. Cell 70, 595–607 (1992). [PubMed: 1505026]
20. Martinelli DC & Fan CM The role of Gas1 in embryonic development and its implications for human disease. Cell Cycle 6, 2650–2655 (2007). [PubMed: 17726382]
21. Fukada S, et al. Molecular signature of quiescent satellite cells in adult skeletal muscle. Stem cells 25, 2448–2459 (2007). [PubMed: 17600112]
22. Martinelli DC & Fan CM Gas1 extends the range of Hedgehog action by facilitating its signaling. Genes & development 21, 1231–1243 (2007). [PubMed: 17504940]
23. Zammit PS, et al. Muscle satellite cells adopt divergent fates: a mechanism for self-renewal? The Journal of cell biology 166, 347–357 (2004). [PubMed: 15277541]
24. Leem YE, et al. Gas1 cooperates with Cdo and promotes myogenic differentiation via activation of p38MAPK. Cell Signal 23, 2021–2029 (2011). [PubMed: 21820049]
25. Lopez-Otin C, Blasco MA, Partridge L, Serrano M & Kroemer G The hallmarks of aging. Cell 153, 1194–1217 (2013). [PubMed: 23746838]
26. Holzenberger M, et al. IGF-1 receptor regulates lifespan and resistance to oxidative stress in mice. Nature 421, 182–187 (2003). [PubMed: 12483226]
27. Lukjanenko L, et al. Loss of fibronectin from the aged stem cell niche affects the regenerative capacity of skeletal muscle in mice. Nature medicine 22, 897–905 (2016).
28. Airaksinen MS & Saarma M The GDNF family: signalling, biological functions and therapeutic value. Nature reviews. Neuroscience 3, 383–394 (2002). [PubMed: 11988777]
29. Luo W, et al. A hierarchical NGF signaling cascade controls Ret-dependent and Ret-independent events during development of nonpeptidergic DRG neurons. Neuron 54, 739–754 (2007). [PubMed: 17553423]
30. Wilhelm SM, et al. Regorafenib (BAY 73–4506): a new oral multikinase inhibitor of angiogenic, stromal and oncogenic receptor tyrosine kinases with potent preclinical antitumor activity. International journal of cancer 129, 245–255 (2011). [PubMed: 21170960]
31. Egner IM, Bruusgaard JC & Gundersen K Satellite cell depletion prevents fiber hypertrophy in skeletal muscle. Development 143, 2898–2906 (2016). [PubMed: 27531949]
32. Lopez-Ramirez MA, Dominguez-Monzon G, Vergara P & Segovia J Gas1 reduces Ret tyrosine 1062 phosphorylation and alters GDNF-mediated intracellular signaling. International journal of developmental neuroscience : the official journal of the International Society for Developmental Neuroscience 26, 497–503 (2008). [PubMed: 18394855]

33. Biau S, Jin S & Fan CM Gastrointestinal defects of the Gas1 mutant involve dysregulated Hedgehog and Ret signaling. Biology open 2, 144–155 (2013). [PubMed: 23429478]
34. Cabrera JR, et al. Gas1 is related to the glial cell-derived neurotrophic factor family receptors alpha and regulates Ret signaling. The Journal of biological chemistry 281, 14330–14339 (2006). [PubMed: 16551639]
35. Sousa-Victor P, et al. Geriatric muscle stem cells switch reversible quiescence into senescence. Nature 506, 316–321 (2014). [PubMed: 24522534]
36. Fry CS, et al. Inducible depletion of satellite cells in adult, sedentary mice impairs muscle regenerative capacity without affecting sarcopenia. Nature medicine 21, 76–80 (2015).
37. Brack AS, et al. Increased Wnt signaling during aging alters muscle stem cell fate and increases fibrosis. Science 317, 807–810 (2007). [PubMed: 17690295]
38. Carlson ME, Hsu M & Conboy IM Imbalance between pSmad3 and Notch induces CDK inhibitors in old muscle stem cells. Nature 454, 528–532 (2008). [PubMed: 18552838]
39. Fontana X, et al. c-Jun in Schwann cells promotes axonal regeneration and motoneuron survival via paracrine signaling. The Journal of cell biology 198, 127–141 (2012). [PubMed: 22753894]
40. Baudet C, et al. Retrograde signaling onto Ret during motor nerve terminal maturation. The Journal of neuroscience : the official journal of the Society for Neuroscience 28, 963–975 (2008). [PubMed: 18216204]
41. Suzuki H, et al. Up-regulation of glial cell line-derived neurotrophic factor (GDNF) expression in regenerating muscle fibers in neuromuscular diseases. Neurosci Lett 257, 165–167 (1998). [PubMed: 9870346]
42. Jin S, Martinelli DC, Zheng X, Tessier-Lavigne M & Fan CM Gas1 is a receptor for sonic hedgehog to repel enteric axons. Proc Natl Acad Sci U S A 112, E73–80 (2015). [PubMed: 25535338]
43. Srinivas S, et al. Cre reporter strains produced by targeted insertion of EYFP and ECFP into the ROSA26 locus. BMC Dev Biol 1, 4 (2001). [PubMed: 11299042]
44. Liu L, Cheung TH, Charville GW & Rando TA Isolation of skeletal muscle stem cells by fluorescence-activated cell sorting. Nat Protoc 10, 1612–1624 (2015). [PubMed: 26401916]
45. Hakim CH, Wasala NB & Duan D Evaluation of muscle function of the extensor digitorum longus muscle ex vivo and tibialis anterior muscle in situ in mice. J Vis Exp (2013).
46. Rozo M, Li L & Fan CM Targeting beta1-integrin signaling enhances regeneration in aged and dystrophic muscle in mice. Nature medicine 22, 889–896 (2016).
47. Subramanian A, et al. Gene set enrichment analysis: a knowledge-based approach for interpreting genome-wide expression profiles. Proc Natl Acad Sci U S A 102, 15545–15550 (2005). [PubMed: 16199517]
48. Zheng X, et al. Low-Cell-Number Epigenome Profiling Aids the Study of Lens Aging and Hematopoiesis. Cell reports 13, 1505–1518 (2015). [PubMed: 26549448]

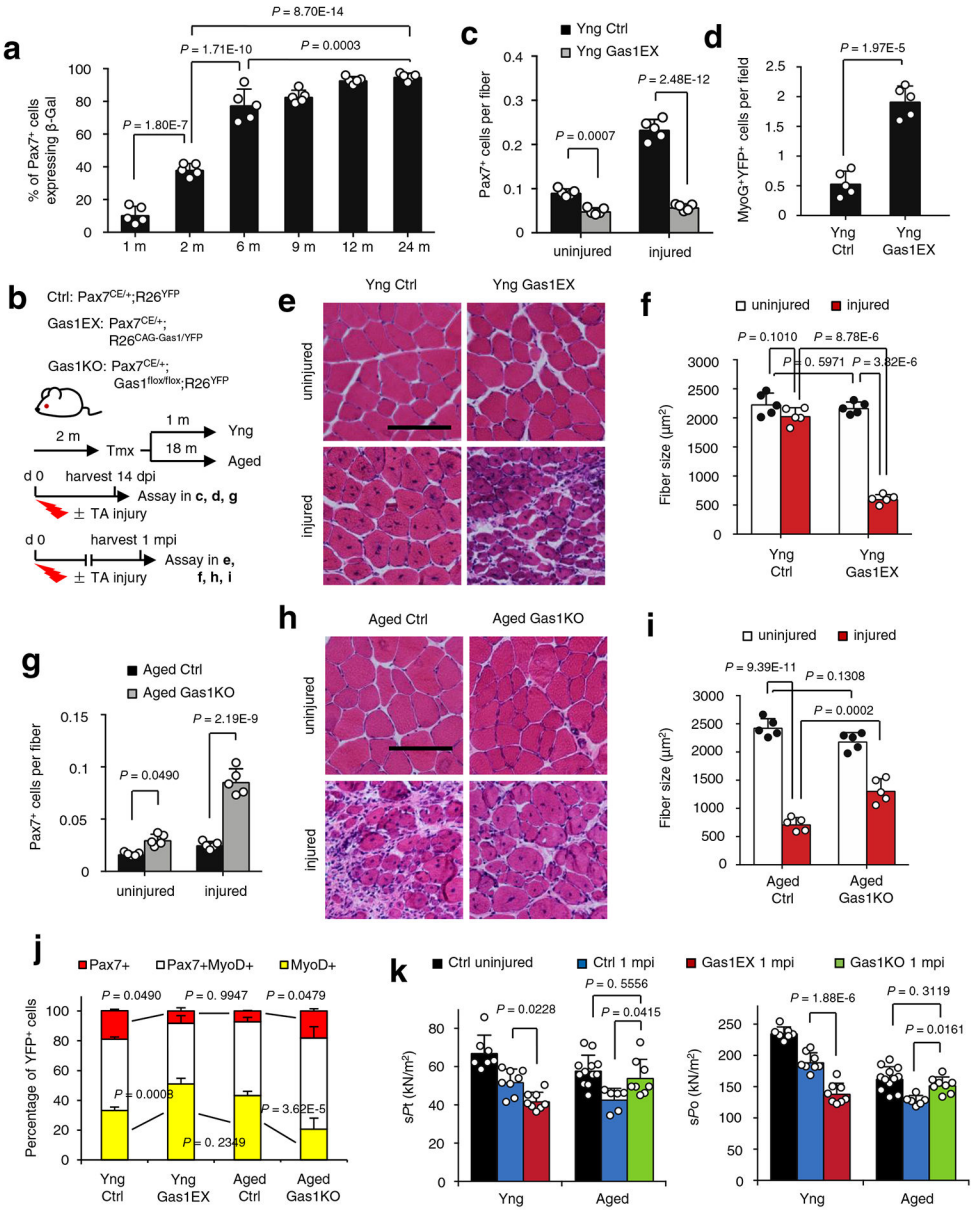

Fig. 1 |. Gas1 associates with aging-like properties of MuSCs.

a, Percentages of β-Gal$^+$Pax7$^+$ in total Pax7$^+$ MuSCs in *Gas1*$^{LacZ/+}$ TA muscles at specified ages (n = 5). **b**, Experimental schemes for young (Yng) control (Ctrl) and Gas1 pan-expression (Gas1EX); aged (Aged) Ctrl and Gas1 knock-out (Gas1KO) mice by *Pax7*^{CE}-directed, Tmx-induced expression; + and – indicate with and without injury, respectively, to the TA muscle. The *R26*^{YFP} reporter allele was included for cell marking. **c**, Averaged Pax7$^+$ MuSCs per fiber for uninjured and injured muscle sections from Yng Ctrl and Gas1EX mice as specified in (**b**) (n = 5). **d**, Averaged MyoG$^+$YFP$^+$ cells per field (1.074 mm^2) of Yng Ctrl and Gas1EX TA muscle sections at 7 d post Tmx without injury (n = 5). **e**, Representative images of TA muscle stained with H&E from Yng Ctrl and Gas1EX mice. **f**, Averaged fiber size from data in (**e**) (n = 5). **g**, Averaged Pax7$^+$ MuSCs per fiber from uninjured and injured muscles from Aged Ctrl and Gas1KO mice (n = 5). **h**, Representative H&E stained images

of TA muscle sections from Aged Ctrl and Gas1KO mice. **i**, Averaged fiber sizes from data in (**h**) (n = 5). **j**, Distribution of self-renewed ($Pax7^{+}MyoD^{-}$), proliferating ($Pax7^{+}MyoD^{+}$), and differentiated ($Pax7^{-}MyoD^{+}$) fractions in single myofiber (SM) cultures after 96 h; myogenic cells are lineage-marked by YFP (n = 3 experiments; ≥ 20 myofibers per condition). For simplicity, legend labeling of negative marker ($Pax7^{-}$ or $MyoD^{-}$) is omitted. **k**, Normalized specific twitch force (*sPt*) and specific maximum tetanic forces (*sPo*) of specified groups (n = 7 for Yng Ctrl uninjured; n = 8 for Yng Ctrl 1mpi, Yng Gas1EX 1mpi, Aged Gas1KO 1mpi; n = 12 for Aged Ctrl uninjured; n = 6 for Aged Ctrl 1mpi). Data are mean ± s.d.; adjusted *P* values are shown; by one-way ANOVA (**a**, **k**); two-way ANOVA (**c**, **f**, **g**, **i**, **j**) and unpaired two-tailed t test (**d**). Scale bars, 150 μm (**e**, **h**).

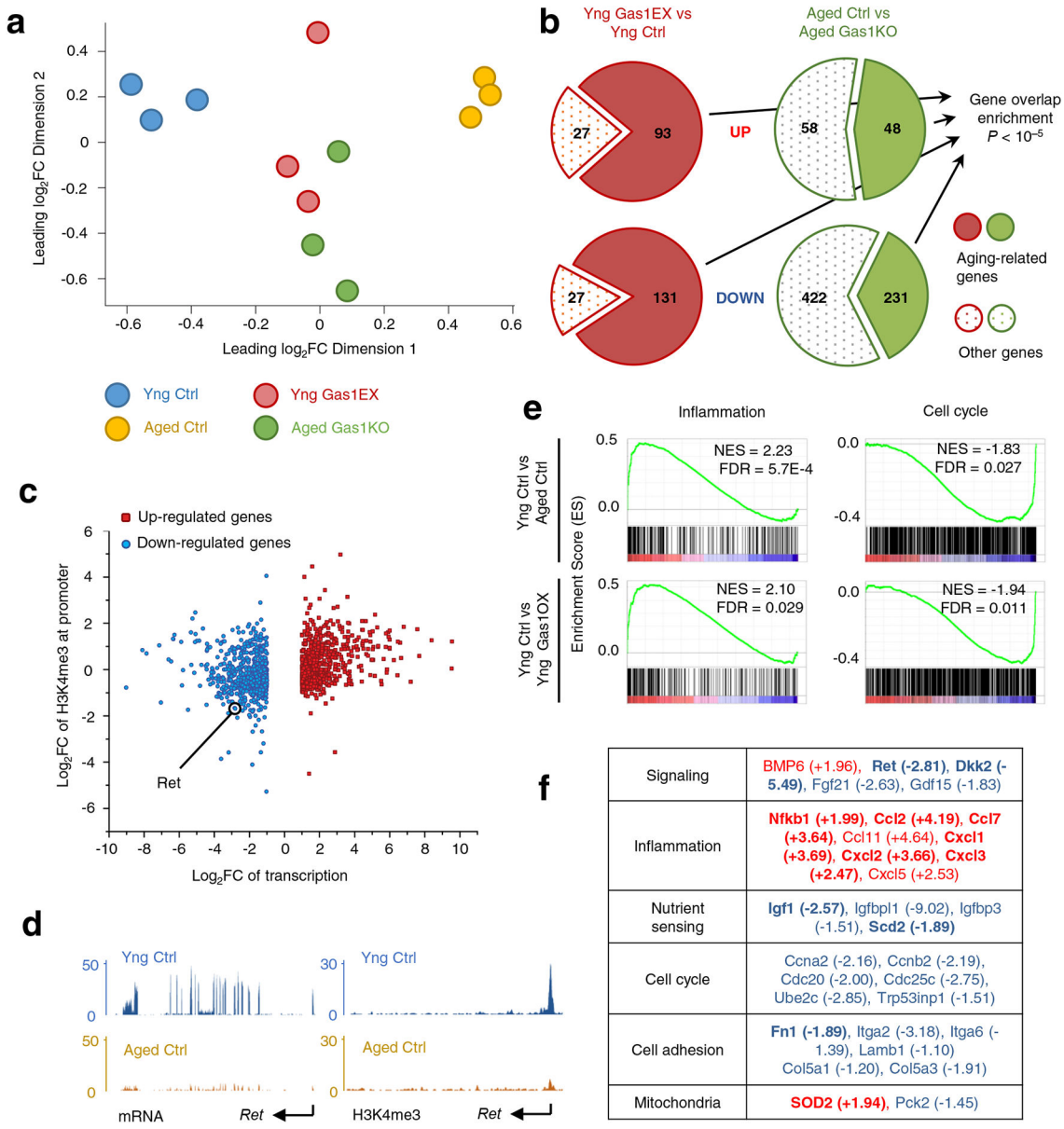

Fig. 2 |. Gas1 mouse models display age-associated molecular signatures of MuSCs.

a, Multidimensional scaling (MDS) plot of transcriptomes of Yng Ctrl, Aged Ctrl, Yng Gas1EX, and Aged Gas1KO MuSCs. **b**, Pie charts for Yng Gas1EX versus Yng Ctrl and Aged Ctrl versus Aged Gas1KO summarize up and down DE genes; aging-related genes in darker shades. Aging-related genes were derived from comparison of Aged Ctrl versus Yng Ctrl. Data were derived from mean of 3 biological replicates using data in **a**; $P < 10^{-5}$; hypergeometric test. **c**, Volcano plots for association between changes in transcription and promoter H3K4me3 mark in Aged and Yng Ctrl MuSCs, derived from means of 3 RNA-seq and 2 ChIP-seq biological replicates. **d**, Representative RNA-seq (left) and H3K4me3 ChIP-seq (right) tracks from Yng Ctrl and Aged Ctrl MuSCs at the Ret locus, using data in **a** and **c** (3 RNA-seq and 2 ChIP-seq biological replicates). **e**, Enrichment for inflammation and cell cycle gene sets by GSEA comparison of Yng Ctrl to Aged Ctrl (top) and Yng Ctrl to Yng

Gas1EX MuSCs (bottom). Data were derived from 3 RNA-seq biological replicates using data in **a**. **f**, Aging hallmark categories for selected DE genes in Aged Ctrl versus Yng Ctrl MuSCs. Log2FCs are indicated; up-regulated in red and down-regulated in blue. DE genes in bold overlap with both Yng Gas1EX versus Yng Ctrl and Aged Ctrl versus Aged Gas1KO comparisons. Genes not in bold overlap with one of the above two comparisons.

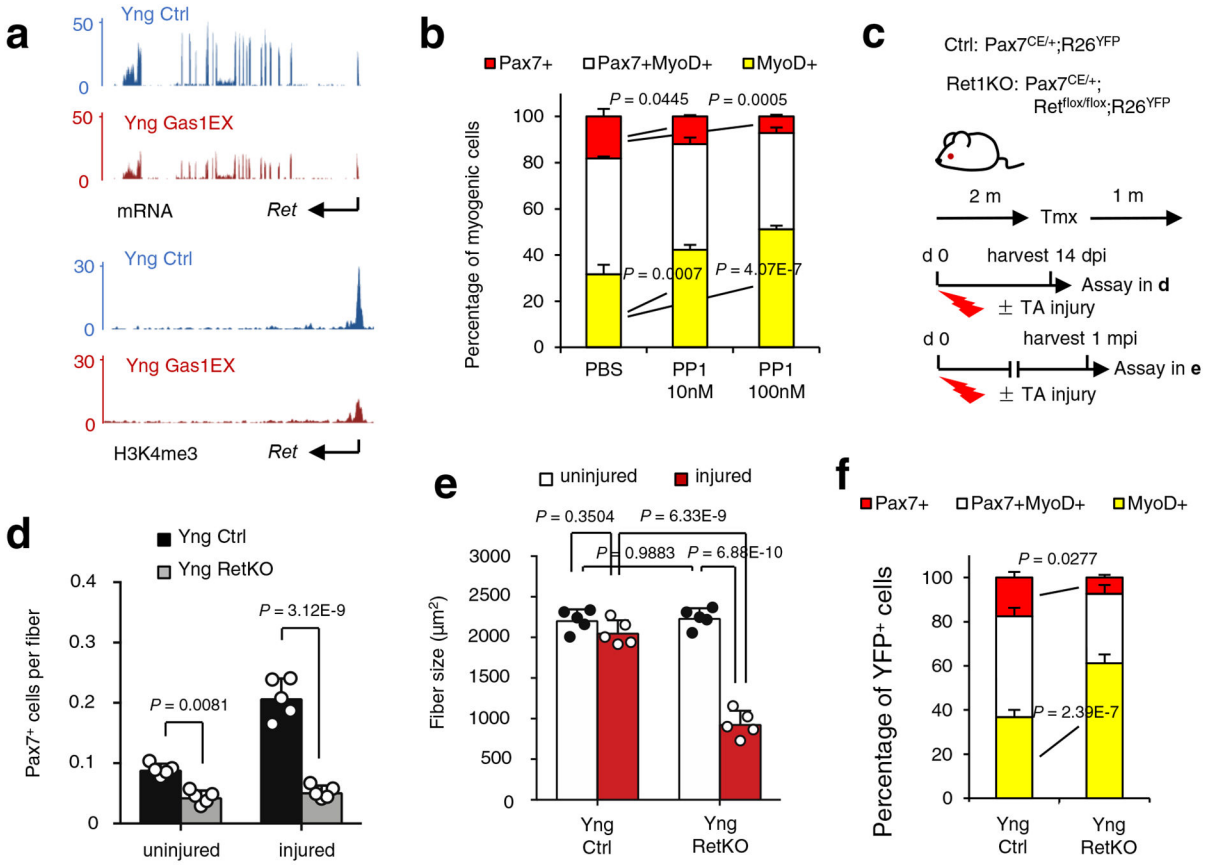

Fig. 3 |. Ret is downstream of Gas1 and required for MuSC self-renewal.

a, RNA-seq (top) and H3K4me3 ChIP-seq (bottom) tracks from Yng Ctrl versus Gas1EX MuSCs at the *Ret* locus, using data in Fig. 2a and **c** (3 RNA-seq and 2 ChIP-seq biological replicates). **b**, SMs isolated from Yng $Ret^{flox/flox}$ mice, cultured for 96 h with or without 1NM-PP1 (PP1, at specified concentrations), stained for Pax7 and MyoD, and quantified for their distributions (n = 3 experiments; ≥ 20 myofibers per condition). **c**, Experimental schemes for Yng Ctrl and RetKO mice; abbreviations same as in Fig. 1b. **d**, Averaged $Pax7^+$ MuSCs per fiber for uninjured and injured TA muscles from Yng Ctrl and RetKO mice (n = 5). **e**, Averaged fiber size for uninjured and injured TA muscles from Yng Ctrl and RetKO mice (n = 5). **f**, Yng Ctrl and RetKO SMs cultured for 96 h, stained for Pax7 and MyoD, and quantified; myogenic cells are lineage-marked by YFP (n = 3 experiments; ≥ 20 myofibers per condition). Data are mean ± s.d.; adjusted *P* values are shown; by two-way ANOVA (**b**, **d**, **e**, **f**). Scale bars, 10 μm (**e**).

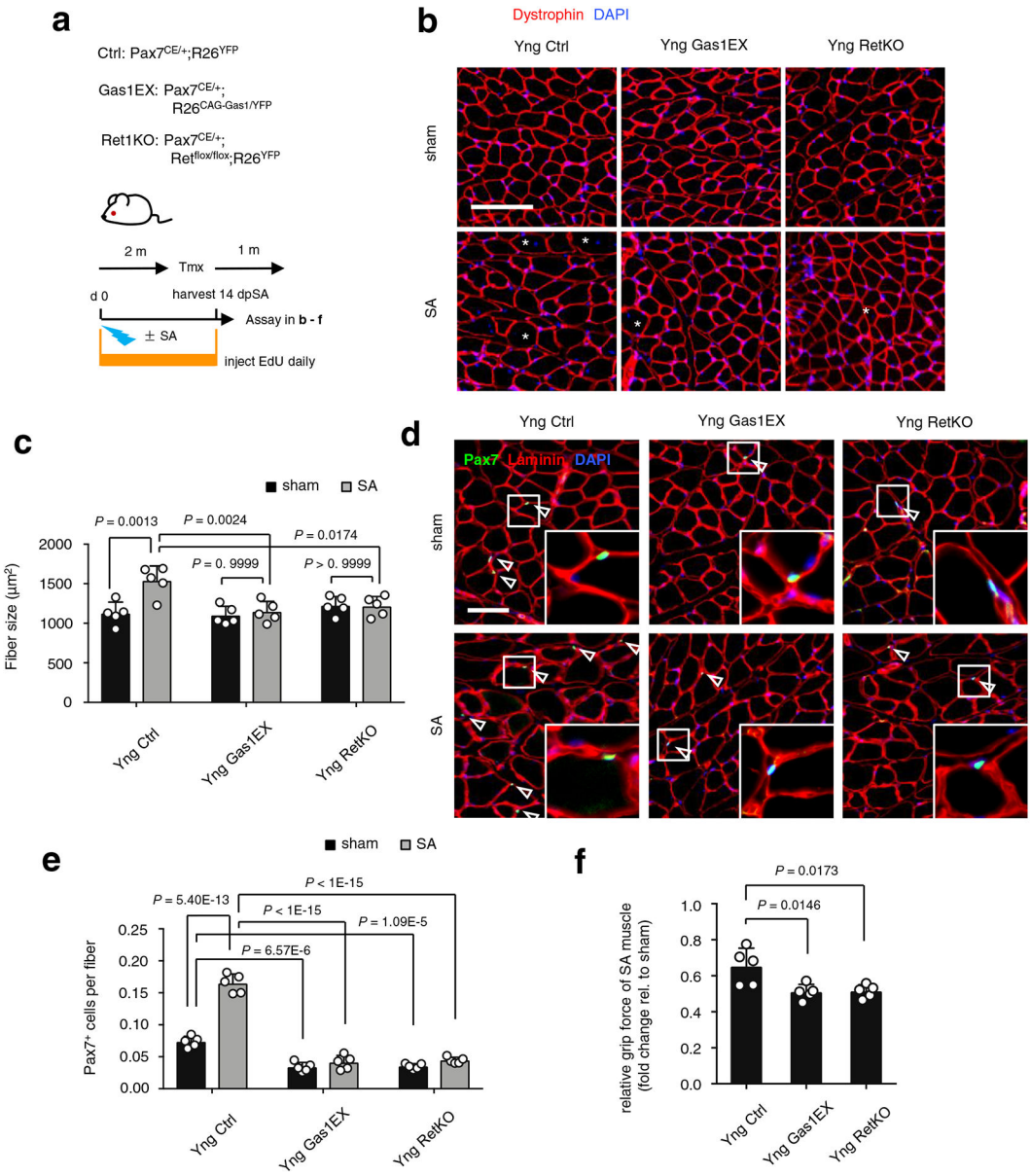

Fig. 4 |. Gas1 and Ret signaling affects compensatory hypertrophic growth of the Plantaris muscle after synergistic ablationn.

a, Experimental scheme for young (Yng) control (Ctrl), Gas1 pan-expression (Gas1EX), and Ret knock-out (RetKO) mice subjected to muscle overload of Plantaris via synergistic ablation (SA) of Soleus and Gastrocnemius muscle; + and – indicate with and without SA, respectively, to the Plantaris muscle. EdU (5 μg/gram body weight) was injected daily for two weeks until harvest. **b**, Plantaris muscles sections from Yng Ctrl, Gas1EX and RetKO mice with or without muscle overload by SA, stained for Dystrophin and DAPI. (n = 5). Asterisk, centrally located myonuclei. **c**, Averaged fiber size from data in (**b**) (n = 5). **d**, Pax7 and Laminin staining on Yng Ctrl, Gas1EX and RetKO Plantaris muscles with or without muscle overload by SA. Arrows, $Pax7^+$ cells. **e**, Averaged $Pax7^+$ MuSCs per fiber for sham control and SA Plantaris muscle sections from Yng Ctrl, Gas1EX and RetKO mice

as in (**d**) (n = 5). **f**, Relative grip strength of hindlimb (fold change compared with sham control) with muscle overload by SA from Yng Ctrl, Gas1EX and RetKO mice (n = 5). Data are mean ± s.d.; adjusted *P* values are shown; by two-way ANOVA (**c**, **e**) and one-way ANOVA (**f**). Scale bars, 100 μm (**b**) and 50 μm (**d**).

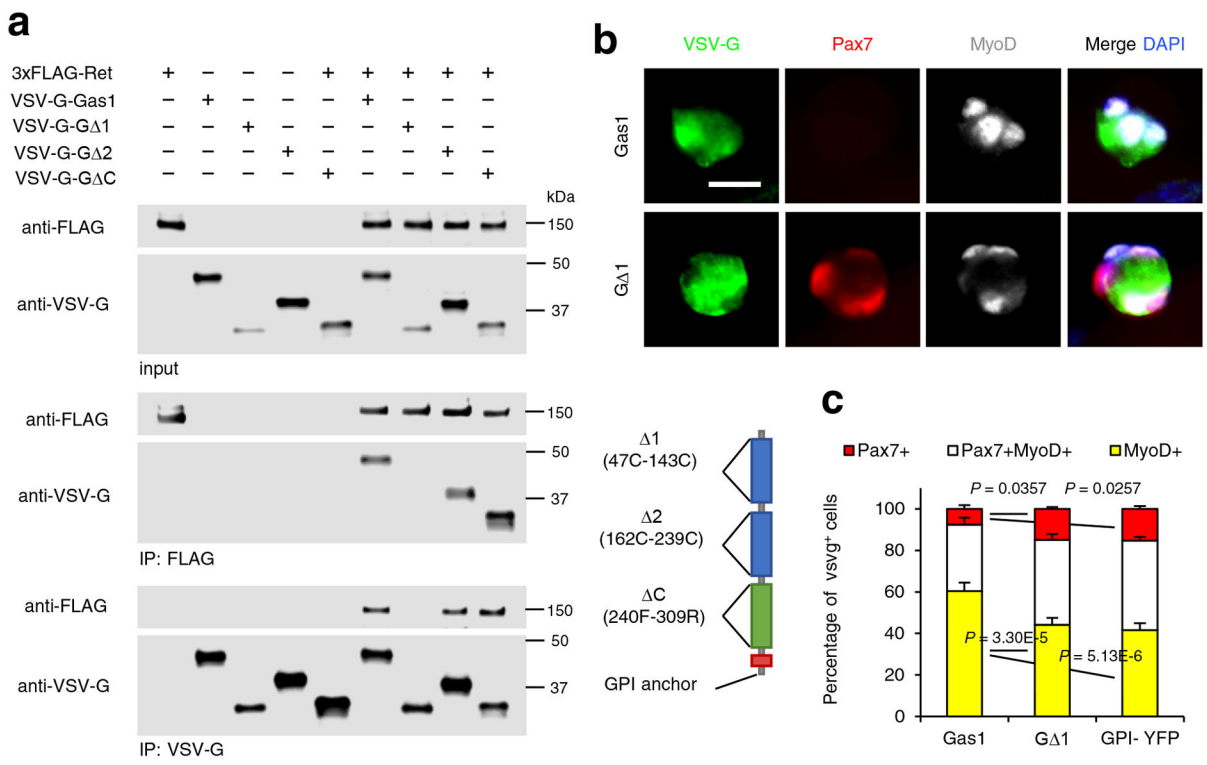

Fig. 5 |. Gas1 interaction with Ret is required for function in MuSCs.

a, Reciprocal co-IPs between 3xFLAG-tagged Ret and VSV-G-tagged full-length and 3 domain-deleted Gas1s (diagrammed at bottom right) expressed in HEK293T cells. Input lysates and FLAG-IPed and VSV-G-IPed fractions are indicated. n = 3 independent experiments with similar results. **b-c**, MuSCs on Yng WT SM transfected with Gas1, Gas1 domain 1-deleted mutant (GΔ1), or GPI-YFP (cultured for 96 h and stained for Pax7 and MyoD (**b**), and quantified for their distribution (**c**) (n = 3 experiments; ≥ 20 myofibers per condition). VSV-G-tagged GPI-YFP served as a control. Data are mean ± s.d.; adjusted *P* values are shown; by two-way ANOVA (**c**). Scale bars, 10 μm (**b**).

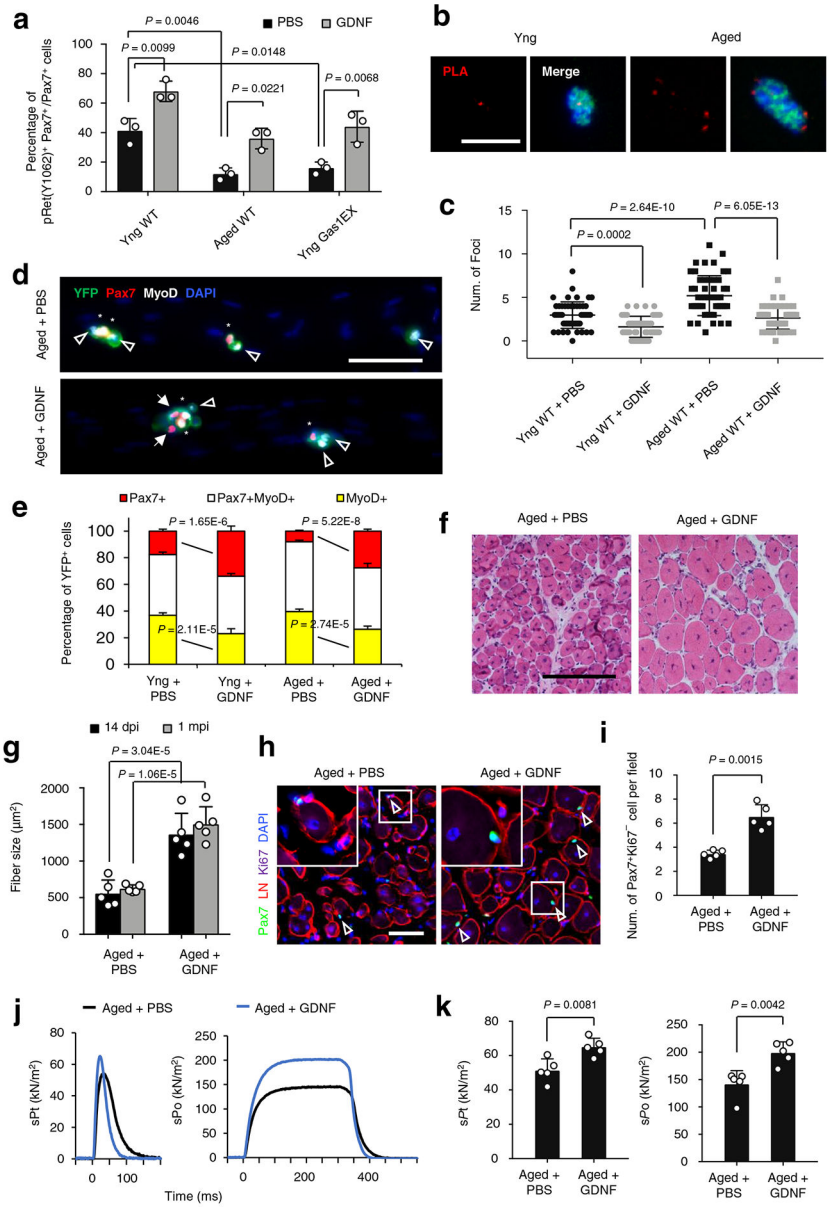

Fig. 6 |. GDNF enhances MuSCs self-renewal and muscle regeneration in aged mice.

a, Percentages of $Pax7^{+}pRet(Y1062)^{+}$ in total $Pax7^{+}$ MuSCs on SMs isolated from Yng or Aged wild-type (WT) or Gas1EX mice and cultured for 24 h with PBS or GDNF (20 ng/ml in PBS) (n = 3 experiments; ≥ 20 myofibers per condition). **b**, Representative images of Gas1:Ret PLA signals (red foci) for MuSCs on Yng or Aged SMs cultured for 24 h; Merge, PLA images merged with Pax7 (green) and DAPI (blue). **c**, Gas1:Ret PLA foci number per MuSC in specified conditions (n = 3 experiments; ≥ 20 myofibers per condition). **d**, Representative images of Aged Ctrl MuSCs on SMs cultured for 96 h with PBS or GDNF (20 ng/ml in PBS) and stained for Pax7 and MyoD. Arrows, $Pax7^{+}MyoD^{-}$ cells; asterisks, $Pax7^{+}MyoD^{+}$ cells; open arrowheads, $Pax7^{-}MyoD^{+}$ cells. **e**, Myogenic distribution for Yng and Aged groups using the assay in (**d**); myogenic cells are lineage-marked by YFP (n = 3 experiments; ≥ 20 myofibers per condition). **f**, Representative images of Aged WT TA

muscles at 1 mpi after intramuscular injections of PBS or GDNF (500 ng; at 2, 4 and 14 dpi) and stained with H&E. **g**, Averaged fiber size from data in **f** (n = 5). **h**, Stained sections from Aged WT TA muscles treated with PBS or GDNF (500 ng; at 2, 4 dpi) at 14 dpi with CTX. **i**, Averaged $Pax7^{+}Ki67^{-}$ (quiescent) MuSCs per field (1.074 mm^2) from data in **h** (n = 5). **j**,**k**, Representative traces of normalized sPt and sPo (**j**) and quantifications (**k**) of Aged WT TA muscles treated with PBS or GDNF at 1 mpi (n = 5). Data are mean ± s.d.; adjusted *P* values are shown; by two-way ANOVA (**a**, **e**, **g**), one-way ANOVA (**c**) and two-sided unpaired t-test (**i**, **k**). Scale bars, 5 μm (**b**), 25 μm (**d**), 150 μm (**f**) and 50 μm (**h**).